Journal of Physics: Conference Series **312** (2011) 082007 doi:10.1088/1742-6596/312/8/082007

Effects of nuclear orientation on fusion and fission process for reactions using ^{238}U target nucleus

Katsuhisa Nishio

Advanced Science Reserch Center, Japan Atomic Energy Agency,
Tokai, Ibraki 319-1195, Japan

E-mail: nishio.katsuhisa@jaea.go.jp

Abstract. Fragment mass distributions for fission after full momentum transfer were measured in the reactions of ^{30}Si,^{34,36}S,^{31}P,^{40}Ar + ^{238}U at bombarding energies around the Coulomb barrier. Mass distributions change significantly as a function of incident beam energy. The asymmetric fission probability increases at sub-barrier energy. The phenomenon is interpreted as an enhanced quasifission probability owing to orientation effects on fusion and/or quasifission. The evaporation residue (ER) cross sections were measured in the reactions of ^{30}Si + ^{238}U and ^{34}S + ^{238}U to obtain information on the fusion probability. In the latter reaction, significant suppression of fusion was implied. This suggests that quasifission has large fraction in the mass-symmetric fission events. The results are supported by a model calculation based on a dynamical calculation using Langevin equation, in which the mass distribution for fusion-fission and quasifission fragments are separately determined.

1. Introduction

Experiments to produce superheavy nuclei (SHN) have been carried out by using heavy ion fusion reactions [1, 2, 3]. Development of a theoretical model to predict cross sections for nuclei located at the extreme end of heavy elements is important for the proper selection of target and projectile as well as the bombarding energy to produce these nuclei. The reaction is considered to proceed in three steps; (1) penetration of the Coulomb barrier between two colliding nuclei, (2) formation of a compound nucleus after the system is captured inside the Coulomb barrier and (3) survival of the excited compound nucleus to produce evaporation residue (ER) against fission (fusion-fission).

The first step, penetrating the Coulomb barrier, is relatively well understood. Enhancing of the capture cross section ($\sigma_{\rm cap}$) relative to the one-dimensional barrier penetration model has been observed at sub-barrier energies, which is explained by the distribution of the Coulomb barrier, as a result of coupling the incident flux to the collective states in the interacting nuclei. Deformation of the target and projectile is another reason for enhancing the capture cross sections. The second process, forming a compound nucleus (fusion probability), is not well understood. A theoretical model must treat the dynamic evolution of a system from the initial touching configuration up to the so called compound nucleus state. In a reaction using a heavy target and projectile, which is the case for the production of the heaviest element, quasifission competes against fusion. Once the fusion cross section is calculated, it is multiplied by the survival probability, which can be determined by a statistical model, to calculate the cross section to produce SHN.

Measurement of the ER cross sections gives information on the fusion probability. However, because of the low production rate for SHN, available data with high statistical accuracy are limited. When a model can treat fusion-fission and quasifission in a consistent framework, such as the unified theory [4], the measurement of fission properties can be another benchmark for testing the model, as fusion-fission and quasifission would have different decay properties.

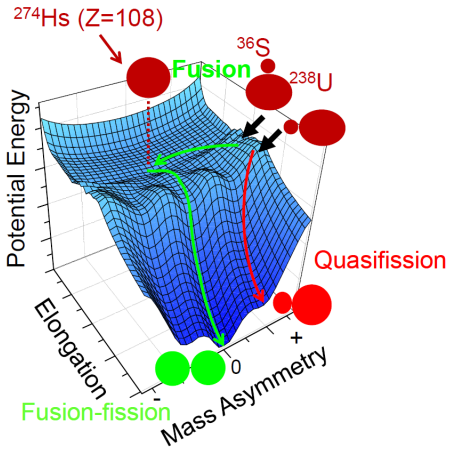

Figure 1. Potential energy for ^{274}Hs produced in the fusion reaction of $^{36}\mathrm{S} + ^{238}\mathrm{U}$.

Fusion reactions using actinide target nuclei are extensively used to investigate SHN. The reasons are (1) a relatively neutron rich SHN compared to the cold fusion reactions are produced, thus the decay properties of these nuclei have information on the structure in the vicinity of the spherically closed-shell at N=184, (2) nuclei having a relatively long half-lives allows a study of the chemical properties, and (3) the cross sections maintain values of a few picobarn even for the production of the heaviest elements [1, 5]. The relatively large cross sections for SHN produced using a ^{48}Ca beam are explained by a high survival probability of the compound nuclei in competition with fission owing to large fission barriers of nuclei in the vicinity of the $N = 184$ shell closure. Another reason could be a higher fusion probability in reactions using actinide targets. Since actinide nuclei are prolately deformed, there exists a configuration at which the projectiles hit the equatorial region of the deformed target nuclei. In this case a compact configuration is achieved and the system may have a larger fusion probability than the reactions using spherical target nuclei such as lead or bismuth.

We have investigated the effects of nuclear orientation on fusion and/or quasifission by measuring the fission fragment mass distributions and the ER cross sections in the reactions using ^{238}U target nuclei to obtain information on fusion probability. The evolution of the nuclear shape from the contact point is largely influenced by the structure of the potential energy and the initial touching point as shown in Fig. 1. At the equatorial collisions, the system has a larger probability to form the compound nucleus, whereas the polar collisions would give higher probability to disintegrate as quasifission. The quasifission is expected to disintegrate through the mass-asymmetric channel.

We also made theoretical calculation based on a dynamical model using Langevin equation to interpret the measured mass distributions. In this calculation, fusion-fission and quasifission fragments are separately determined, and thus we can estimate the fusion cross section. The ER cross section is then determined from the fusion cross section multiplied by the survival probability of the excited compound nucleus which is calculated by a statistical model. A comparison of the ER cross section with the experimental data will be given to see if the Langevin description gives a appropriate value of fusion probability.

2. Experimental details

2.1. In-beam fission measurement

The mass distributions and cross sections of fission fragments in the reactions of ^{30}Si,^{34,36}S,^{31}P,^{40}Ar + ^{238}U were measured using beams supplied by the tandem accelerator of the Japan Atomic Energy Agency (JAEA) in Tokai, Japan. The experimental set-up and the analysis method were described in [6].

Beam energies were changed from above-barrier to sub-barrier values. The beam intensities were typically from 0.1 to 1.0 p-nA. The ^{238}U target was prepared by electrodeposition of UO_2 on a 90-μg/cm^2 thick nickel backing. Both fission fragments (FFs) were detected in coincidence by position-sensitive multiwire proportional counters (MWPCs). The detectors were located on both sides of the target each at a distance of 211 mm. We determined the emission angles of both fragments as shown in Fig.2. The detector center was placed at $\theta_1 = -61.0°$ for MWPC1 and $\theta_2 = +90.0°$ for MWPC2 with $\phi_1 = \phi_2 = 0°$ in the reactions of ^{30}Si,^{34,36}S,^{31}P + ^{238}U. The angles of $\theta_1 = -72.0°$ and $\theta_2 = +72.0°$ were chosen in the ^{40}Ar + ^{238}U reaction. The MWPCs covered the emission angular range of $\theta_1 = \theta_2 = \pm 25.0°$ around the detector center.

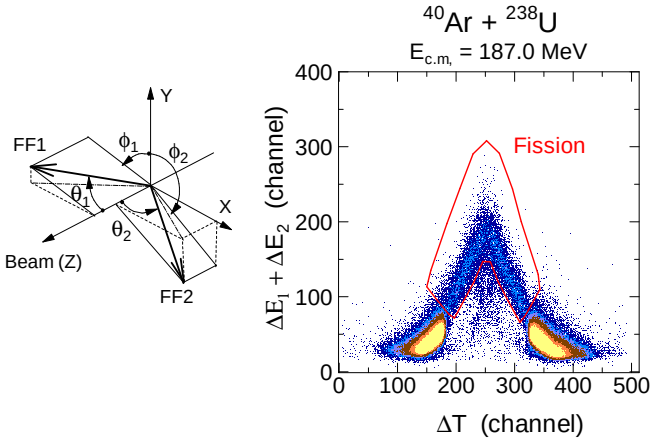

Figure 2. (Left) Definition of emission angles for both fission fragments. (Right) Coincidence events plotted on ΔT and $\Delta E_1 + \Delta E_2$ in the reaction of ^{40}Ar+^{238}U. Fission events are marked.

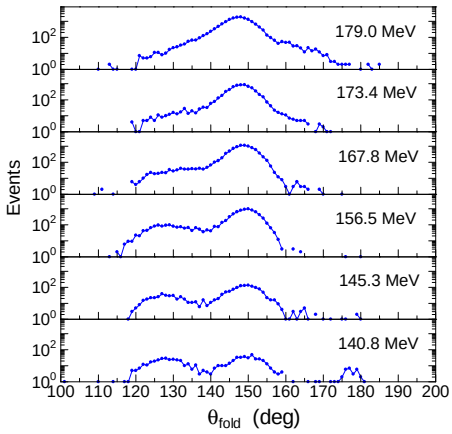

Figure 3. Distribution for folding angle of fission fragments produced in the ^{30}Si + ^{238}U reaction. The beam energy in the laboratory frame is indicated.

The time difference, ΔT, between the signals from MWPC1 and MWPC2 was measured. The charges induced in both MWPCs contain information on the energy deposition ΔE_1 and ΔE_2 of particles traversing the detectors and were recorded. In the two dimensional spectrum of ΔT versus $\Delta E_1 + \Delta E_2$ (Fig.2), fission events were well separated from elastically scattered projectile-target events.

Fission events occurring after complete transfer of the projectile momentum to the composite system (full momentum transfer (FMT) fission) are separated from those fission events following nuclear transfer. These latter events occur when fissile targets like ^{238}U are irradiated. Figure. 3 shows the folding angle distributions for fission fragments produced in the ^{30}Si + ^{238}U reaction. The FMT fissions are located around $\theta_{\rm fold} = 148°$ at the incident energy of $E_{\rm lab} = 179.3$ MeV and around $\theta_{\rm fold} = 150°$ at the lowest energy 140.8 MeV. Fission following nucleon transfer has a larger folding angle than the FMT fission in the high energy region of $E_{\rm lab} = 179.0$ MeV, as seen in the tail on the spectra which extends over $\theta_{\rm fold} = 160°$. In the low energy region, nucleon transfer fission is observed with a smaller folding angle of $\theta_{\rm fold} = 120° - 140°$ than the

FMT fission. These trends are explained by the angular dependence of the transfer reactions, which preferentially occur at grazing angles. The FMT fission fragments were separated from the nuclear transfer fission on the ($\theta_{\rm fold}$, $\phi_{\rm sum}$) plane, and used for the analysis.

2.2. Evaporation residue measurement

Measurements of ER cross sections were carried out in the reactions of ^{30}Si + ^{238}U and ^{34}S + ^{238}U. The experiments were performed at the linear accelerator UNILAC and the velocity filter SHIP at GSI in Darmstadt. The SHIP set-up was essentially the same as described in [2]. The ^{30}Si beam was extracted from a 14 GHz ECR ion source using isotopically enriched material, ^{30}SiO (99.5% isotopic enrichment). A $^{34}SO_2$ gas with a 99 % isotopic enrichment was used to extract the ^{34}S beam. Average beam intensities at the target position were typically 0.7−1.0 $p\mu$A for ^{30}Si and 2.0−2.5 $p\mu$A for ^{34}S. The beam had a pulse structure of 5.0 ms width at 50 Hz repetition frequency. Details of the experiments are described in [7, 8].

For the ^{30}Si + ^{238}U run, the uranium targets were prepared by evaporation of isotopically depleted $^{238}UF_4$ and condensation on a carbon backing. In the experiment of ^{34}S + ^{238}U, the targets were prepared by sputtering the depleted ^{238}U metal on a carbon backing.

The efficiency of SHIP was determined using a Monte Carlo calculation. We obtained a value of 11 % and 15 % for ^{30}Si + ^{238}U and ^{34}S + ^{238}U, respectively.

In the focal plane of the SHIP, ERs and their subsequent α decay and/or spontaneous fission (sf) were detected by a position sensitive 16-strip Si PIPS detector (stop detector) with an active area of 80 mm × 35 mm. The energy resolution for fully stopped α's was typically 25∼26 keV (FWHM). Escaping α particles or a complementary fission fragments were detected by a 'box detector' which covered 85% of the area of the backward hemisphere. Timing detectors were located in front of the silicon detector array to distinguish signals from implanted ERs or background particles from radioactive decays in the stop detector. The correlated events is identified primarily based on a coincidence of the positions of implanted ER, subsequent α decays and/or sf.

3. Experimental results

3.1. In-beam fission measurement

The cross sections for the FMT fissions ($\sigma_{\rm fiss}$) of ^{30}Si + ^{238}U are shown in Fig.4(a) as a function of the center-of-mass energy, $E_{\rm c.m.}$, as well as an excitation energy of the compound nucleus, E^*. The cross section was obtained by fitting the fragment angular distribution in the center-of-mass angle to a function described in [9] and integrating the fitted curve over the solid angle. The fission cross section is almost equal to the capture cross section ($\sigma_{\rm cap}$).

In order to see the effects of nuclear properties on the capture cross sections, we show in Fig. 4(a) the calculation using the coupled-channels code, CCDEGEN [10]. The dotted curve is the result without considering any collective properties or deformation of the target and projectile (one-dimensional barrier penetration model). The dashed curve is the result which takes into account the prolate deformation of ^{238}U with $(\beta_2, \beta_4) = (0.275, 0.050)$ [11]. The calculation reproduces within the error the experimental data down to $E_{\rm c.m.}$ =129.0 MeV. The solid curve is the result additionally taking into account the coupling to the 3^- state at 0.73 MeV in ^{238}U [12] (β_3 =0.086 [13]), which reproduces also the data at the lowest incident energy of 125.0 MeV. Low Coulomb barrier for the polar collisions, as marked in the upper part of Fig. 4, is the main reason for the enhancement of the capture cross section at the sub-barrier energies relative to the one-dimensional barrier penetration model.

The fission cross sections for ^{34}S + ^{238}U are shown in Fig. 5(a). The data are compared with the coupled-channels calculations. The assumptions given to draw the dotted and dashed curves are the same as in Fig.4(a). To reproduce the lowest data point at $E_{\rm c.m.}$ =140.0 MeV, couplings

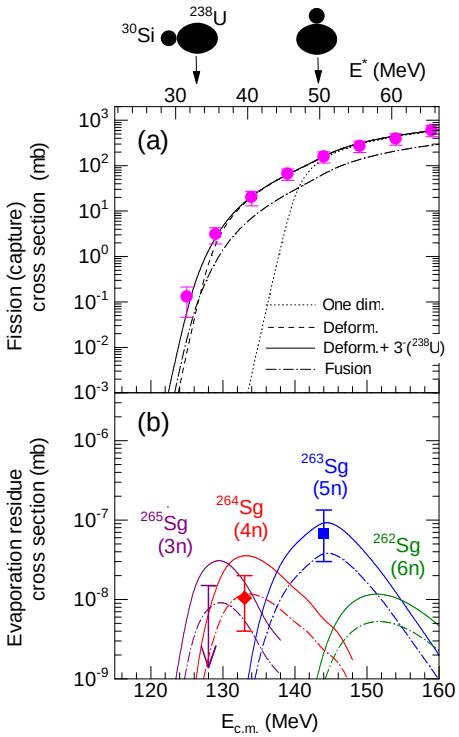

Figure 4. (a) Cross sections for FMT fission and (b) evaporation residue cross sections for $^{30}\mathrm{Si}+^{238}\mathrm{U}$. Curves are the model calculations (see text).

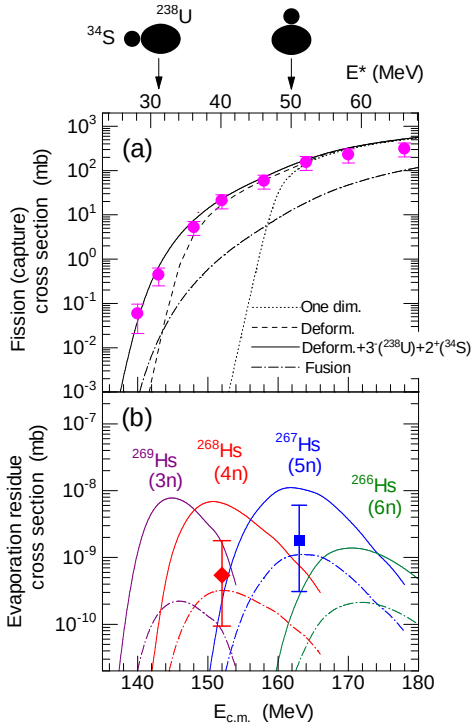

Figure 5. (a) Cross sections for FMT fission and (b) evaporation residue cross sections for $^{34}\mathrm{S}+^{238}\mathrm{U}$. Curves are the model calculations (see text).

to 3^- state (0.73 MeV) in ^{238}U and to the 2^+ state (2.13 MeV [12]) in ^{34}S (β_2 =0.25 [14]) are taken into account (solid curve).

Figure 6(a) shows the mass distributions for the FMT fissions in the $^{30}\mathrm{Si}+^{238}\mathrm{U}$ reaction. To draw the mass distribution, we assumed that the mass distributions do not depend on $\theta_{\mathrm{c.m.}}$. The distributions are Gaussian with mass symmetry in the energy range from $E_{\mathrm{c.m.}}=139.0$ MeV to 154.0 MeV. The shape of the distributions, however, are different for the sub-barrier energies at $E_{\mathrm{c.m.}}=134.0$ and 129.0 MeV. They have asymmetric component around $A_{\mathrm{L}}/A_{\mathrm{H}}\approx 90/178$. The difference of the mass distribution at the lowest energy data is characterized also by the standard deviation σ_{m} as indicated in each panel of Fig. 6(a). The value increases from 28.1±1.0 u (139.0 MeV) to 37.5±1.0 u (134.0 MeV). Considering the measured ER cross sections (Fig. 4(b)), as discussed in the following, we conclude that the asymmetric fission channel originates from quasifission.

The mass distributions in the $^{34}\mathrm{S}+^{238}\mathrm{U}$ reaction are shown in Fig. 6(b). At the highest energy of 170.0 MeV, the distribution is Gaussian with mass symmetry. The σ_{m} value of the spectrum, however, is far larger than the one for $^{30}\mathrm{Si}+^{238}\mathrm{U}$. Toward the low incident energy, the asymmetric fission yield increases sharply around the mass asymmetry $A_{\mathrm{L}}=68$ and $A_{\mathrm{H}}=204$. The mass asymmetry corresponds to the fragments near the double-closed shell nuclei, ^{78}Ni and ^{132}Sn (see Fig. 1). A similar observation was made in the study of the reaction $^{36}\mathrm{S}+^{238}\mathrm{U}\rightarrow{}^{274}\mathrm{Hs}^*$ [6]. The phenomenon was interpreted by the effects of nuclear orientation on fusion and/or quasifission. At the sub-barrier energy, projectiles collide only on the polar sides of the ^{238}U nucleus. In this case the reaction starts from a distant contact point with a large charge-center distance, which results in a larger quasifission probability than the reactions starting from

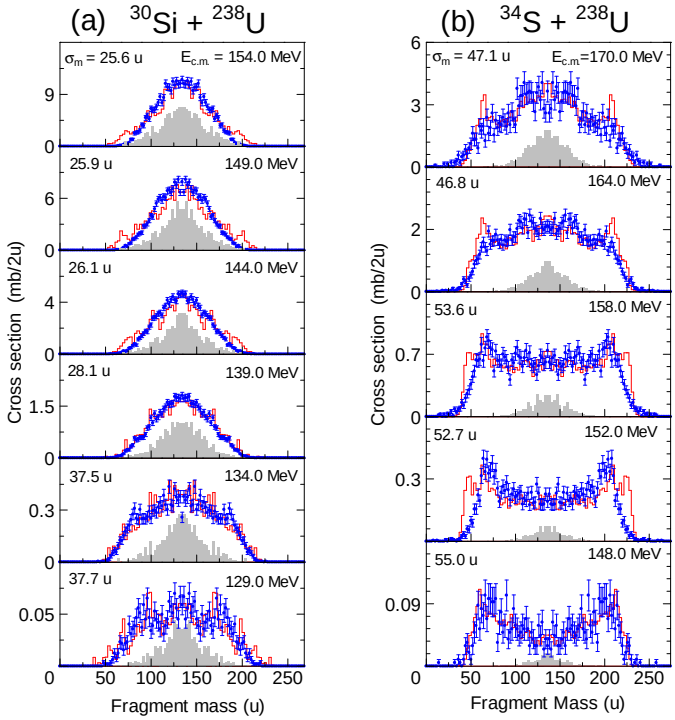

Figure 6. Fragment mass distributions for FMT fissions of the reactions (a) $^{30}\mathrm{Si}+^{238}\mathrm{U}$ and (b) $^{34}\mathrm{S}+^{238}\mathrm{U}$. Histograms shows a model calculation. The calculated fusion-fission spectrum is shown by the filled area. Reaction energy in the center-of-mass system and the standard deviation σ_{m} of the measured spectrum are shown.

the equatorial collisions (see Fig. 1).

Figure 7 shows the mass distributions in the reactions using different projectiles of ^{30}Si,^{31}P,^{36}S and ^{40}Ar. The excitation energy of a compound nucleus is shown in each section of the figure. For a fixed excitation energy, a yield for an asymmetric fission channel increases with projectile charge, showing that quasifission probability increases due to the larger Coulomb repulsive force in the reaction process. The enhanced quasifission yield toward the low incident energy are observed for all the reactions owing to the orientation effects.

In the reactions of $^{34}\mathrm{S}+^{238}\mathrm{U}$ (Fig.6(b)), $^{36}\mathrm{S}+^{238}\mathrm{U}$ (Fig.7) and $^{40}\mathrm{Ar}+^{238}\mathrm{U}$ (Fig.7), the quasifission mass asymmetries are nearly the same, and centered around $A_{\mathrm{L}}/A_{\mathrm{H}} \approx$ 68/204, 74/200 and 76/202, respectively. According to the mass asymmetry parameter $\alpha = (A_{\mathrm{H}} - A_{\mathrm{L}})/(A_{\mathrm{H}} + A_{\mathrm{L}})$ defined by the light (L) and heavy (H) fragment masses, they corresponds to 0.50, 0.46 and 0.45. These mass asymmetry are closely correlated to the fission channel formed by the shells near the double-closed shell nuclei, ^{78}Ni and ^{208}Pb (see Fig.1). This channel is the same as observed in reactions using heavier projectiles bombarded to actinide target nuclei [15], where the reactions of $^{48}\mathrm{Ca}+^{238}\mathrm{U}$, $^{244}\mathrm{Pu}$, $^{248}\mathrm{Cm}$ produce asymmetric fission centered at $A_{\mathrm{H}} \approx 210$ ($\alpha = 0.42 \sim 0.46$).

The observed mass asymmetry in the quasifission for $^{30}\mathrm{Si}+^{238}\mathrm{U}$ is $\alpha = 0.33$ ($A_{\mathrm{L}}/A_{\mathrm{H}} \approx 90/178$). The value is significantly smaller than those obtained for $^{34}\mathrm{S}$,$^{36}\mathrm{S}$,$^{40}\mathrm{Ar}+^{238}\mathrm{U}$. The asymmetric fission channel in the $^{31}\mathrm{P}+^{238}\mathrm{U}$ reaction, $\alpha = 0.40$ ($A_{\mathrm{L}}/A_{\mathrm{H}} \approx 81/188$), also does not fit the shells of ^{78}Ni/^{208}Pb. The potential energy landscape of ^{268}Sg produced by $^{30}\mathrm{Si}+^{238}\mathrm{U}$ has almost the same structure as ^{274}Hs produced by $^{36}\mathrm{S}+^{238}\mathrm{U}$ (see Fig. 5 in [6]). The observation of the different mass asymmetry indicates the difference in the evolution of nuclear shape

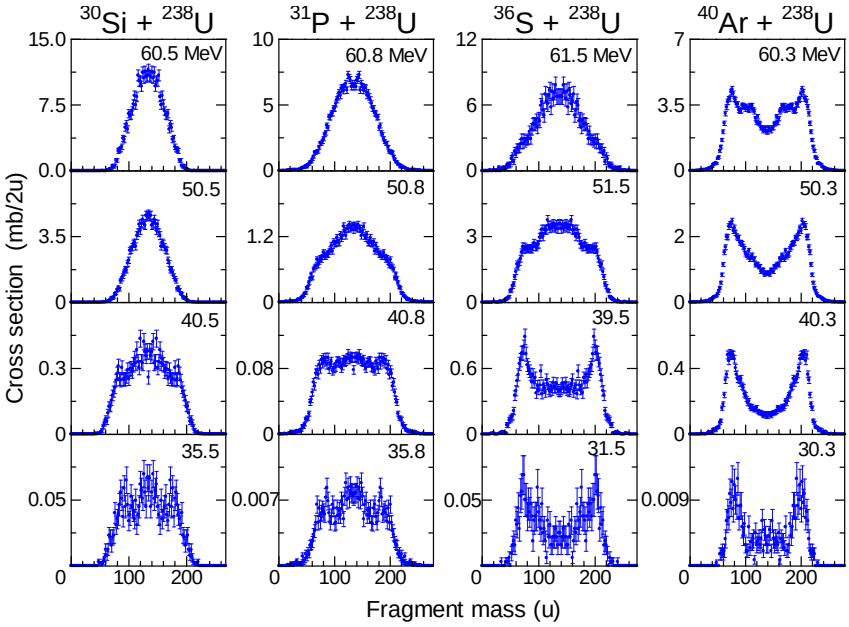

Figure 7. Fission fragment mass distributions in the reactions of ^{30}Si,^{31}P,^{36}S,^{40}Ar + ^{238}U. The excitation energy E^* of a compound nucleus is shown in each spectrum.

in quasifission.

3.2. Evaporation residue measurement

The measurement of ER cross sections in the fusion of ^{30}Si + ^{238}U was carried out from April 8 to May 1, 2006. We used three different beam energies of $E_{\rm c.m.} = 144.0$, 133.0 and 128.0 MeV, which correspond to the anticipated maximum cross sections of $5n$-, $4n$-, and $3n$-evaporation channels. Details of the experimental results are described in [7].

At 144.0 MeV, a beam dose of 1.8×10^{18} was accumulated. We observed three α-decay chains starting from ^{263}Sg($5n$). We obtained the cross section of 67^{+67}_{-37} pb. At the sub-barrier energy of $E_{\rm c.m.} = 133.0$ MeV, we observed three recoil-sf correlations with a beam dose of 4.0×10^{18}. The half-life was determined to be $120^{+126}_{-\ 44}$ ms for the sf decay. The nucleus was assigned to the spontaneously fissioning isotope ^{264}Sg ($4n$). The cross section for the three ^{264}Sg sf events was $10^{+10}_{-\ 6}$ pb. At the lowest beam energy of 145.5 MeV, no decay events were measured with a beam dose of 1.7×10^{18}. An upper cross section limit was determined to be 15 pb at 68 % confidence level (one event would have had a cross section of 8.2 pb). Measured cross sections and/or the cross section limit are shown in Fig. 4(b).

Production of hassium isotopes in the fusion of ^{34}S + ^{238}U was carried out from January 17 to February 8, 2009. Two different beam energies of $E_{\rm c.m.} = 163.0$ and 152.0 MeV were chosen, corresponding to the maximum $5n$- and $4n$-evaporation cross sections. Details of the experimental results are described in [8].

At $E_{\rm c.m.} = 163.0$ MeV, a beam dose of 4.8×10^{18} was accumulated. We observed one decay chain, which we assign to the production of ^{267}Hs as shown in Fig. 8. The cross section for ^{267}Hs was determined to be $1.8^{+4.2}_{-1.5}$ pb as plotted in Fig. 5(b). The value agrees with 2.5 pb measured in [16]. At the sub-barrier energy of $E_{\rm c.m.} = 152.0$ MeV, a beam dose of 1.2×10^{19} was accumulated. In this irradiation, one decay chain was identified, as shown in Fig.8. We assigned the decay chain starting from the new isotope ^{268}Hs. The 9749-keV α-decay was followed by the sf of ^{264}Sg which was produced directly in the $4n$-evaporation in fusion of ^{30}Si + ^{238}U [7]. The

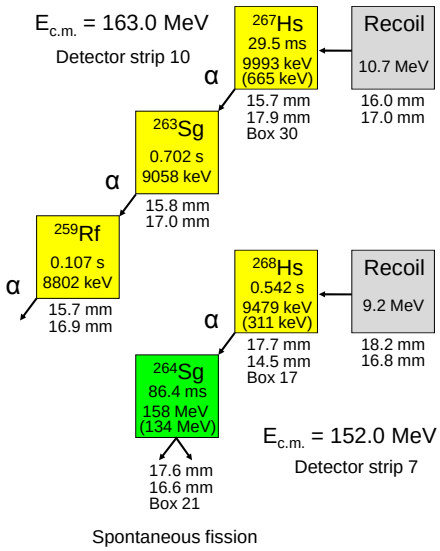

Figure 8. Decay chains observed in the $^{34}\mathrm{S} + ^{238}\mathrm{U}$ reaction. For the details, see [8]

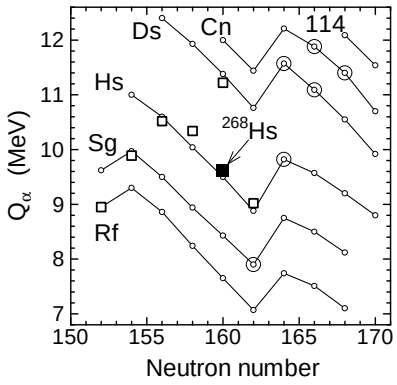

Figure 9. Alpha-decay Q-values of even-even nuclei in the region of N=162. Present new isotope ^{268}Hs is shown. Lines represent the theory [17]. Double circles represent nuclei and their daughter products which could be studied in the reactions $^{34,36}\mathrm{S} + ^{248}\mathrm{Cm}$,$^{244}\mathrm{Pu}$ and $4n$-evaporation channels.

obtained cross section $0.54^{+1.3}_{-0.45}$ pb is shown in Fig. 5(b).

The α-decay Q value, Q_α, of ^{268}Hs is shown in Fig. 9 together with those for the other isotopes. The theoretical data [17] are also shown, which predicts the decreasing Q_α value toward the deformed neutron-shell at $N = 162$. The present data for ^{268}Hs fits perfectly into the systematics as well as theoretical value.

4. Discussion

For a quantitative analysis of the mass distributions, we performed a model calculation combining the coupled channels method and a dynamical description of the reaction based on the three-dimensional Langevin equation [18]. The dynamical calculation based on the Monte Carlo method was used for describing the reaction paths in the potential energy landscape. The two-center shell model was used to calculated the potential energy of a nucleus whose shape is defined by z (charge center distance), δ (deformation) and α (mass asymmetry). The deformation of the reaction partners and their orientation in the reaction plane was considered. The coupled channels method was first used to compute the penetration probability of the Coulomb barrier for a fixed orientation angle. The dynamical calculation was then started from the shape at contact configuration for each orientation. Fusion is defined as the case when the trajectory enters inside the local energy minimum corresponding to the compound nucleus, whereas quasifission is defined as disintegration without reaching the minimum.

The calculated distributions of FMT fragments for $^{30}\mathrm{Si} + ^{238}\mathrm{U}$ are represented by the histograms in Fig. 6(a). The model reproduces the general shape of the distribution as well as the feature of the appearance of the asymmetric fission channel and increase of the standard deviation σ_m at the sub-barrier energies. The calculated fusion-fission events in this model are shown by the filled areas in Fig. 6(a). It is Gaussian with mass symmetry, and the standard deviation of the spectrum σ_m is nearly constant with 21∼25 u in the entire energy range. The value is significantly smaller than $37 \sim 38$ u for the measured distributions at the sub-barrier energies of 129.0 and 134.0 MeV. Furthermore the calculated fusion-fission spectrum does not show any asymmetric fission channels. The results support the observed asymmetric fission to be quasifission. In the calculation, we can determine the fusion probability P_fus as the ratio of

fusion-fission events to the FMT fission events. By multiplying the $P_{\rm fus}$ to capture cross section ($\sigma_{\rm cap}$), a fusion cross section $\sigma_{\rm fus}$ is obtained. The results for $^{30}{\rm Si}+^{238}{\rm U}$ are shown by the dash-dotted curve in Fig. 4(a).

The same calculation was made in the $^{34}{\rm S}+^{238}{\rm U}$ reaction as shown in Fig. 6(b). The results reproduce the measured distribution, especially transition from symmetric to asymmetric mass distributions with different incident energy is well reproduced. The $\sigma_{\rm m}$ value in the calculated fusion-fission spectrum is 16−20 u, which is nearly the same as the $^{30}{\rm Si}+^{238}{\rm U}$ reaction. The value is about factor two less than those for the measured distribution. A remarkable difference between $^{30}{\rm Si}+^{238}{\rm U}$ and $^{34}{\rm S}+^{238}{\rm U}$ reactions is the fusion-fission yield among the FMT fissions. Even in the symmetric mass region, the yield drops significantly in the case of ^{34}S projectile. For $^{34}{\rm S}+^{238}{\rm U}$, the fusion-fission probability in the symmetric-fission channel, which is determined by decomposing the spectrum into two Gaussian distributions representing symmetric and asymmetric channels, is 0.15 at $E_{\rm c.m.}=164.0$ MeV. The value is 0.42 for $^{30}{\rm Si}+^{238}{\rm U}$ at $E_{\rm c.m.}=144.0$ MeV (We assume $^{30}{\rm Si}+^{238}{\rm U}$ has only symmetric fission channel in this energy). The fusion cross sections $\sigma_{\rm fus}$ for $^{34}{\rm S}+^{238}{\rm U}$ are shown in Fig. 5(a) by the dash-dotted curve.

To see if the above model is appropriate to estimate the fusion probability, $P_{\rm fus}$, a statistical model code HIVAP [19] was used to calculate the ER cross sections by inputting the fusion cross sections for $^{30}{\rm Si}+^{238}{\rm U}$ (dash-dotted curve in Fig. 4(a)), and the results are compared with the experimental data Fig.4(b). The calculation reproduces the cross sections for ^{263,264}Sg within errors as well as the cross section limit for ^{265}Sg. Similarly, the model can account for the cross sections for ^{267,268}Hs produced in the fusion of $^{34}{\rm S}+^{238}{\rm U}$ as shown in Fig. 5(b). If we assume all the fragments were arising from the compound nucleus fission, the ER cross sections would have values shown by the solid curves in Fig. 4(b) or Fig. 5(b). Apparently, this assumption conflicts the cross sections of ^{264,265}Sg and ^{267,268}Hs.

It is shown in the calculated ER cross sections for $^{34}{\rm S}+^{238}{\rm U}$ in Fig. 5(b) that the probability for quasifission after the capture process becomes larger toward the low bombarding energy, demonstrating the orientation effects. It is consistent with the experimental data of ^{268}Hs and ^{267}Hs.

In spite of the reduced fusion probability to produce SHN using heavier projectiles, ^{34}S, our cross section calculations reveal a considerable yield for producing relatively neutron rich nuclei at energies below the Bass barrier, when targets of deformed actinide nuclei are used. Figure 5(b) shows the cross sections for the $3n$ evaporation channel, ^{269}Hs. The cross section is expected to be comparable to the one for the $4n$ evaporation residue, ^{268}Hs. By applying fusion reaction at the energy below the Bass barrier, the new isotopes $^{274-277}$Ds (N=164−167) could be produced in the reactions $^{34,36}{\rm S}+^{244}{\rm Pu}$ in $3n$–$4n$ evaporation channels or $^{278-281}$Cn (N=166−169) in $^{34,36}{\rm S}+^{248}{\rm Cm}$ reactions also in $3n$–$4n$ channels. Alpha decay from these nuclei would populate isotopes of hassium and seaborgium, from which the isotopes ^{272,273}Hs (N=164 and 165) and ^{268,269}Sg (N=162 and 163) are not yet known. Similarly, isotopes of odd elements could be produced in reactions with ^{34,36}S beams and a ^{243}Am target. The ERs and their daughter nuclei includes new isotopes of ^{273,275,276}Rg (N=162, 164 and 165) and ^{269,271,272}Mt (N=160, 162 and 163).

The knowledge of synthesis and decay properties of the nuclei discussed above is especially important. First, they build a bridge between the well established, but relatively neutron deficient nuclei produced in cold fusion reactions and those with higher neutron number produced in hot fusion, which are not connected to known nuclei, because their α-decay chains are terminated by sf. Second, the α-decay Q-values of these new nuclei together with those for the known nuclei provide information on the increased binding energy at the deformed shells with Z =108 and N =162. Due to the large gaps in the single particle energies, increased Q_α values are expected beyond these neutron and proton numbers. In Fig. 9 the predicted Q_α values

not observed so far are marked by double circles.

5. Conclusions

The mass distributions for FMT fission fragments in the reactions of ^{30}Si,^{34,36}S,^{31}P,^{40}Ar + ^{238}U were measured at bombarding energies around the Coulomb barrier. The probability of asymmetric fission increases at the sub-barrier energy. The phenomenon is interpreted as the enhanced quasifission probability, which represents orientation effects on fusion and/or quasifission. The ER cross sections were measured in the reactions of ^{30}Si + ^{238}U and ^{34}S + ^{238}U to obtain information on fusion probability $P_{\rm fus}$. The $P_{\rm fus}$ decreased significantly for the latter reaction, thus showing the enhanced quasifission probability. The conclusion was consistent with the theoretical model calculation which is based on the Langevin equation and takes into account the orientation of the deformed nucleus ^{238}U, in which fusion-fission and quasifission are separately determined. In spite of the significantly low fusion probability at the sub-barrier energy, there are fusion probabilities large enough to produce $3n$- and $4n$-evaporation residues. In the combination between ^{34,36}S projectile and several actinide target nuclei, totally 18 new isotopes could be produced as ER or α-decay descendants. They are located in the region of elements from seaborgium to copernicium with neutron numbers $\geq$162 so that the gap between the known nuclei produced in cold and hot fusion reactions could be filled.

The investigations were accomplished with the collaborators of H. Ikezoe, S. Mitsuoka, Y. Nagame, I. Nishinaka, K. Tsukada, K. Tsuruta (JAEA), S. Hofmann, D. Ackermann, V.F. Comas, Ch.E. Düllmann, S. Heinz, J.A. Heredia, F.P. Heßberger, J. Khuyagbaatar, B. Kindler, I. Kojouharov, P. Kuusiniemi, B. Lommel, R. Mann, M. Mazzocco, M. Schädel, H.J. Schött, B. Sulignano (GSI), Y. Aritomo (JAEA,FLNR), K. Hagino, K. Hirose, T. Ohtsuki (Tohoku University), A.G. Popeko, A. Svirikhin, A.V. Yeremin(FLNR), S. Antalic, S. Saro (Comenius University), A. Gorshkov, R. Graeger, A. Türler, A. Yakushev (TU München), Y. Watanabe (KEK), Z. Gan (IMP), We are grateful to W. Hartmann, J. Steiner, H.G. Burkhard, and J. Maurer of GSI.

We would like to thank the UNILAC staff and the crew of the JAEA tandem accelerator facility for preparation and operation of the beams. This work was supported by a Grant-in-Aid for Scientific Research of the Japan Society for the Promotion of Science.

References

[1] Yu.Ts. Oganessian, J. Phys. G **34**, R165 (2007).
[2] S. Hofmann and G. Münzenberg, Rev. Mod. Phys. **72**, 733 (2000).
[3] K. Morita *et al.*, J. Phys. Soc. Jpn. **73**, 1738 (2004).
[4] V. Zagrebaev and W. Greiner, J. Phys. G, **31** 825 (2005).
[5] S. Hofmann *et al.*, Eur. Phys. J. A **32**, 251 (2007).
[6] K. Nishio *et al.*, Phys. Rev. C **77**, 064607 (2008).
[7] K. Nishio *et al.*, Eur. Phys. J. A **29**, 281 (2006).
[8] K. Nishio *et al*,. Phys. Rev. C, **82** 024611 (2010).
[9] R. Vandenbosch and J.R. Huizenga, *Nuclear Fisson* (Academic Press, New York, 1973).
[10] modified version of the CCFULL code, K. Hagino *et al.*, Computer Phys. Comm. **123**, 143 (1999).
[11] K. Nishio *et al.*, Phys. Rev. Lett. **93**, 162701 (2004).
[12] R.B. Firestone *et al*,. *Table of Isotopes Eighth Edition* (JohnWiley & Sons, Inc.)
[13] R.H. Spear *et al.*, At. Data Nucl. Data Tables, **42**, 55 (1989).
[14] S. Raman *et al.*, At. Data Nucl. Data Tables, **36**, 1 (1987).
[15] M.G. Itkis *et al.*, Nucl. Phys. **A787**, 150c (2007).
[16] Yu.A. Lazarev *et al.*, Phys. Rev. Lett. **75**, 1903 (1995).
[17] I. Muntian *et al*,. Acta. Phys. Pol. B **34** 2073 (2003).
[18] Calculation is based on a model in Y. Aritomo, Phys. Rev. C, **80**, 064604 (2009), but effects of nuclear orientaion was taken into account (Y. Aritomo *et al.*, to be submitted).
[19] W. Reisdorf and M. Schädel, Z. Phys. A **343**, 47 (1992).